Applied Energy 358 (2024) 122555

Contents lists available at ScienceDirect

Applied Energy

journal homepage: www.elsevier.com/locate/apenergy

A hybrid deep learning approach for remaining useful life prediction of lithium-ion batteries based on discharging fragments

Yunpeng Liu [a,b,c], Bo Hou [d], Moin Ahmed [c], Zhiyu Mao [b,e,*], Jiangtao Feng [a,*], Zhongwei Chen [b,c,**]

[a] Department of Environmental Science & Engineering, School of Energy and Power Engineering, Xi'an Jiaotong University, Xi'an, 710049, China
[b] Power Battery & System Research Center, Dalian Institute of Chemical Physics, Chinese Academy of Sciences, Dalian 116023, China
[c] Department of Chemical Engineering, University of Waterloo, 200 University Avenue West, Waterloo, ON N2L 3G1, Canada
[d] School of Physics and Astronomy, Cardiff University, The Parade, Cardiff, CF24 3AA, Wales, UK
[e] College of Chemistry and Life Sciences, Zhejiang Normal University, Jinhua 321004, China

GRAPHICAL ABSTRACT

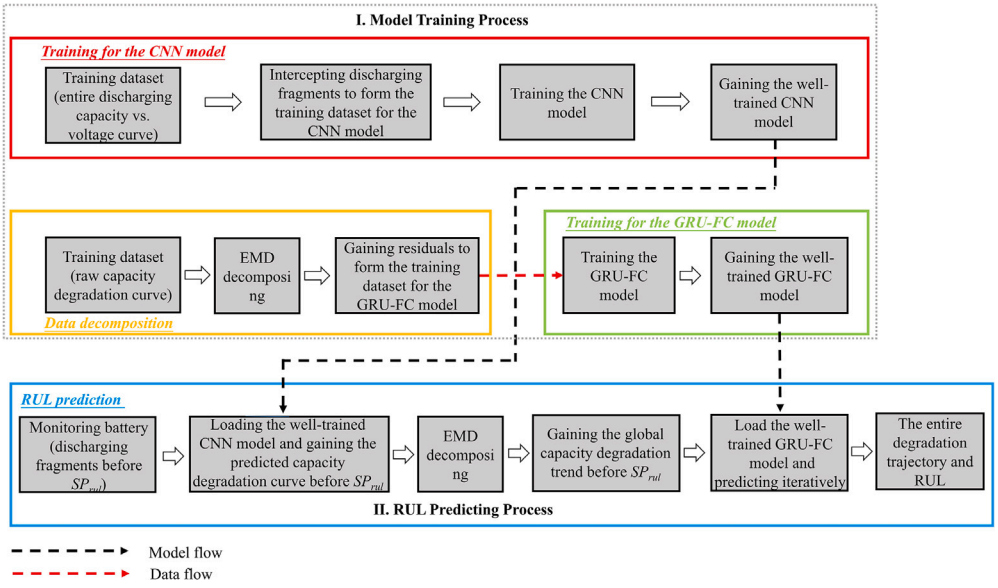

ARTICLE INFO

Keywords:
Lithium-ion battery
Remaining useful life
Discharging fragment
Deep learning
Decomposition noise

ABSTRACT

Accurate remaining useful life (RUL) estimation is crucial for the normal and safe operations of lithium-ion batteries (LIBs). Traditionally, every cycle's maximum discharging capacity should be measured and then serve as a model input to predict iteratively the degradation trajectory. Unfortunately, full discharge stages are not always present in practice. Herein, this study presents a hybrid approach consisting of signal decomposition and deep learning to overcome the above limitations. Firstly, for the collected discharging fragments, the convolutional neural networks model predicts every cycle's maximum discharging capacity which combines to form a predicted capacity degradation curve before the start point of RUL prediction. Then, via empirical mode decomposition, this curve's global degradation trend is extracted and serves as the subsequent model

* Corresponding authors.
** Corresponding author at: Department of Chemical Engineering, University of Waterloo, 200 University Avenue West, Waterloo, ON N2L 3G1, Canada.
E-mail addresses: zhymao@zjnu.edu.cn (Z. Mao), fjtes@xjtu.edu.cn (J. Feng), zhwchen@uwaterloo.ca (Z. Chen).

https://doi.org/10.1016/j.apenergy.2023.122555
Received 19 June 2023; Received in revised form 30 November 2023; Accepted 21 December 2023
Available online 5 January 2024

input. Finally, the entire degradation trajectory and RUL value could be inferred based on the well-trained gated recurrent unit-fully connected model. The superior prediction performance of the proposed method is verified on two open battery datasets. All the estimation errors can be maintained within 7.0% based on the discharging fragment of the ~20% capacity ratio ranges from 40% to 60% of the degradation data. This result illustrates the promising accuracy and robustness of the developed LIBs RUL estimation method, especially for not full discharge process in practice.

1. Introduction

Lithium-ion batteries (LIBs) are excellent rechargeable power sources powering our daily lives, including drones, mobile phones, electric vehicles, and satellites, due to their lightweight, high energy and power density, wide working range, and fast charging rate [1]. However, the aging problem related to the capacity degradation of LIBs may cause decreased performance and catastrophic accidents in severe cases. Therefore, people need to establish a battery management system (BMS) to accurately and robustly monitor running status, which is mainly divided into three indicators: remaining useful life (RUL) [2], state of charge (SOC) [3], and state of health (SOH) [4]. The RUL of a battery is defined as the number of remaining charge–discharge cycles before its running status reaches the failure threshold, which could help the user to develop a feasible plan to optimize the batteries' working status, so the LIBs' RUL prediction attracts more and more attention [5]. However, the highly complicated and nonlinear electrochemical process, and inconstant degradation mechanism of LIBs, hinder the enhancement of the prediction performance of BMS [6].

To meet these challenges, many model-based and data-driven approaches have been developed [7,8]. Typically, model-based approaches could be divided into two main categories, i.e., the mechanism model and the mathematical model [9]. The mechanism model either analyzes physical and chemical reactions to describe the capacity aging process of LIBs (such as the equivalent circuit model), or fits charges transfer and mass transfer processes by the partial differential equations [10]. Although the high prediction accuracy could be realized, the expensive computing cost and intricate mechanisms still obstacles their applications. On the other hand, the mathematical model, such as the empirical model, employs filtering algorithms to provide a non-destructive means of characterizing batteries to achieve RUL and SOH prediction [11]. However, the prediction accuracy of mathematical approaches is sensitive to external environmental conditions and model parameters [12]. Therefore, data-driven approaches have attracted attention owing to their strong robustness and adaptability to the nonlinear capacity degradation phenomenon of LIBs.

Data-driven approaches such as the support vector regression (SVR) [13], gaussian process regression (GPR) [14], and relevance vector machine (RVM) [15], have been developed to use information from historical time-series battery dataset (the changes of battery's voltage, current, capacity and surface temperature) to predict its future performance, i.e., RUL and SOH. For example, Yang et al. [16] proposed an RUL prediction method for LIBs based on an integration of ensemble empirical mode decomposition (EEMD), gray wolf optimization (GWO), and SVR to predict global capacity degradation and capacity regeneration in battery capacity time series. Zhang et al. [17] decomposed battery capacity data by variational modal decomposition (VMD) and applied dual GPR models to predict the SOH of LIBs. Chen et al. [18] proposed a hybrid algorithm that combines the broad learning system (BLS) with the RVM to predict the LIBs RUL, suitable for the time series field with noise and few data features. However, prediction accuracy of these data-driven approaches still do not meet the need of all life cycle stages [19]. Moreover, appropriate feature engineering is also challenging to implement in general machine learning algorithms [20].

Artificial neural network (ANN), could potentially resolve the above issues because the high-level and underlying information from large-scale dataset can be extracted [21]. For instance, the recurrent neural network (RNN) and its derivatives have shown good performance in predicting SOH and RUL, which are typical task of temporal sequence. Li et al. [22] employed long short-term memory (LSTM) for SOH and RUL estimation of LIBs, which avoided the gradient vanishing problem of the traditional RNN. Lu et al. [23] further utilized gated recurrent unit (GRU), a simplified LSTM, to constitute the framework to predict the battery capacity degradation trajectories under both fixed and random battery operating conditions. Tong et al. [24] put forward a hybrid approach for RUL prediction, which was composed with adaptive dropout LSTM and Monte Carlo Simulation, and this approach exhibited relatively low data requirement and good prediction accuracy. However, the desired predicted accuracy of the aforementioned RUL prediction heavily depends on the precondition, that the every cycle's maximum discharging capacity before the starting point of RUL prediction (SP_{rul}), needs to be known [25,26]. In other words, every discharging process should start at the upper voltage limit (UVL) and end at the lower voltage limit (LVL). Unfortunately, full discharge states such as mobile phones or electric vehicles often do not occur in practical applications. Therefore, it is a worthwhile research to predict RUL based on discharging fragments. Zhang et al. [27] constructed a hybrid parallel residual convolutional neural network (CNN) with a 4.15% test error for RUL prediction based on the sparse data corresponding to only 20% charging capacity. On the other hand, Chen et al. [28] designed an empirical-data hybrid driven approach to realize the RUL prediction of LIBs based on battery charging voltage fragment, which utilized the prior knowledge and historical dataset efficiently. Recently, Tian et al. [29] proposed a novel CNN model to reconstruct the complete charging or discharging curve based on the randomly chosen fragments. Hence, maximum discharging capacity of every cycle could be acquired via a relative low-cost model, which provided us new vision for RUL prediction.

Due to the randomness of capacity regeneration, the measured trajectory of LIBs could be influenced by noise signal, which could reduce the RUL prediction accuracy. Furthermore, suppose the noise signal is considered. In this case, the complexity of the BMS would increase when dual or more complex data-driven models are employed to forecast the over-detailed degradation changes [16]. Besides, the noise originating from the predicted maximum discharging capacity of every cycle before SP_{rul}, would weaken the forecast of the global degradation trend. Recently, Cheng et al. [30] employed the empirical mode decomposition (EMD) to reduce the impact of capacity regeneration and other factors, and then accurately separated the low-frequency degradation trend from high-frequency capacity noise. These results demonstrate EMD method has a simple structure, high robustness, and applicability for different LIBs.

Herein, a new hybrid data-driven approach is proposed to precisely and economically predict the LIBs RUL. This hybrid method is named CEG and composes the CNN model, EMD method, and GRU network with fully connected layers (GRU-FC).

The primary innovations and contributions of this paper are elaborated as follows:

(1) The CNN model is applied to gain the corresponding maximum discharging capacity of the discharging fragments. This process could not only guarantee the fragments' voltage ranges do not have to be fixed or complete, but also provide maximum discharging capacity of every cycle before SP_{rul}.
(2) To gain the global capacity degradation trend before SP_{rul}, the EMD method is employed to decompose the predicted outcomes from the above CNN model. This process could decrease the distraction originating from capacity regeneration, and then those

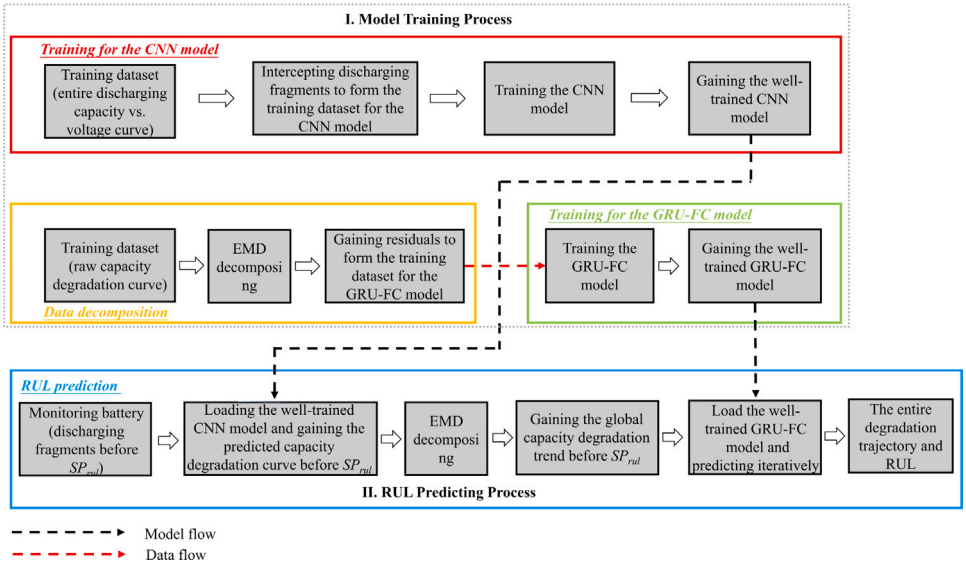

Fig. 1. The framework of the CEG approach for the RUL prediction.

extracted residuals would be beneficial to improve the accuracy of the subsequent RUL prediction model.

(3) The GRU-FC model is employed to predict the RUL based on the above decomposed residual. The simplified temporal model could efficiently grasp the global capacity degradation features of this type of battery. Finally, the hybrid approach consisting of CNN model, EMD method, and GRU-FC model, achieves a more suitable RUL forecast even though the original data is discharging fragments.

The rest of this paper is organized as follows: Section 2 introduces the methodologies of the proposed CEG approach. Section 3 presents the prediction performance of this approach via utilizing two case studies, and Section 4 summarizes our results and makes conclusions.

2. Model overview

2.1. RUL prediction approach framework

As shown in Fig. 1, the whole approach framework consists of two main stages: the model training process and the RUL predicting process.

(1) Model training process: The training dataset are composed of the LIBs' measured capacity degradation data under different operational conditions, and the battery aging index, including the voltage and discharge capacity, is extracted. Firstly, the entire discharging curves are split randomly into fragments to form the training dataset of the CNN model. Next, the CNN model is trained to find the mapping relationship between the discharging fragments and their corresponding maximum discharging capacity. Then, via the EMD method, the residuals of the raw capacity degradation curves are decomposed to form the training dataset of the GRU-FC model. Finally, the GRU-FC model is trained to grasp the capacity degradation features of this type of battery.

(2) RUL predicting processing: After collecting the test battery's discharging fragments before SP_{rul}, the well-trained CNN model is loaded, and then exports the maximum discharging capacity of every cycle, which combines into a predicted capacity degradation curve before SP_{rul}. Then, via the EMD method, this curve is decomposed to the predicted global capacity degradation trend before SP_{rul} which serves as the input of the well-trained GRU-FC model. Via constant iterations, the subsequent capacity degradation trajectory could be predicted, and thus the RUL value also could be inferred.

2.2. CNN model

The overall CNN model is designed based on previous work with some modifications, as shown in Fig. 2 [29]. It consists of five layers: the 1D convolutional (Conv1d), maximum pool (MaxPool1d), adaptive maximum pooling layer (AdaptiveMaxPool1d), fully connected (FC), and dropout layers. Firstly, this architecture starts with the stacked convolutional layer and pooling layer, and the local features of the discharging fragments could be extracted efficiently. Then, two FC layers and a dropout layer are employed to normalize those features. The last FC layer also serves as the output layer to output the predicted entire discharging curve. In this work, 16, 8, and 8 filters for the three Conv1d layers are used in sequence, respectively. Meanwhile, the window size, padding size, and moving step of convolutional filters are 3, 1, and 1, respectively. A non-linear activation function (ReLU) is also utilized to avoid potential vanishing gradient problems. The MaxPool1d layers could concentrate features, and the kernel size of the first two pooling layers is 3. The last one is the AdaptiveMaxPool1d layer, which coordinates the data size requirement and summarizes spatial information. Then, the extracted features are sent to the first FC layer (148 neurons), followed by the ReLU activation function. The dropout layer (dropout rate is set at 20%) is used to deal with the output originating from the first FC layer to prevent the over-fitting problem. Finally, the output layer is also a FC layer, and its amount of neurons is decided by the length of the predicted discharging curve. The detailed structure data of CNN model are listed in Table S1.

The Adam algorithm is employed to update model parameters iteratively. The batch size is 500. During the CNN model training process, 30% of the training dataset is randomly selected as a validation dataset and used to improve the model's prediction accuracy. After training for 50 000 epochs, the CNN model with the lowest validation loss is picked up and used for predicting the test batteries' maximum discharging capacity. Overfitting problem is repressed via early stopping approach in which the patience is set to 10. Namely, the training process would be stopped, once the valid loss does not continue to decrease in 10 iterative steps.

2.3. Data pre-processing method for CNN model

The voltage ($V(\tau)$) and current ($I(\tau)$) are measured during the constant current discharging. According to the Ah counting, the discharging capacity (Q) could be calculated as follow:

$$Q(V) = \int_{V(\tau)=V}^{V(\tau)=V_{\text{upper}}} |I(\tau)| d\tau \tag{1}$$

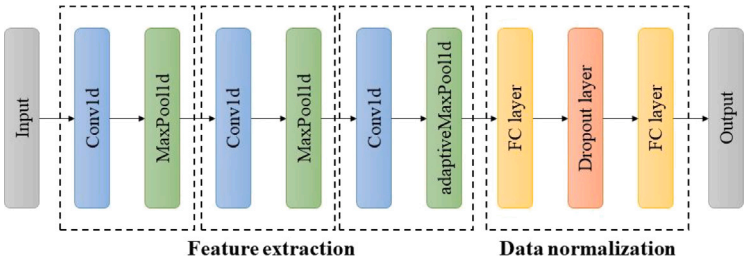

Fig. 2. The architecture of the developed CNN model.

where the V_{upper} represents the *UVL*, and the $Q(V)$ represents the discharging curve at the giving voltage range $[V_{upper}, V_{upper} - \Delta V, \ldots, V_{upper} - N\Delta V]$, where ΔV is voltage step, $N = (V_{upper} - V_{lower})/\Delta V$, and V_{lower} represents the discharging ending voltage. Therefore, the discharging curve could form a matrix with two columns and $(N+1)$ rows. Because the full discharge does not happen very often process is not usually fully carried out in practice, the discharging fragments are utilized in this study. Therefore, the intercepted fragment is $\left[\left[V_s, V_{s+1}, \cdots, V_{s+a}\right], \left[Q_s - Q_{s-1}, Q_{s+1} - Q_{s-1}, \cdots, Q_{s+\alpha} - Q_{s-1}\right]\right]$, $(1 \le \alpha \le N-1,\ 2 \le s \le N - \alpha + 1)$, which is made up of the voltage and discharging capacity sequence. Meanwhile, the corresponding predicted label should be the entire discharging curve $Q(V)$. According to the optimized results of the reported literature [29], the sequence length of voltage is set to 300 mV ($V_s - V_{s+\alpha}$ = 300 mV). Meanwhile, the starting-point capacity value of this fragment should be set to 0 because the fragment is independent of the original discharging curve. The ending-point capacity value of this fragment could be computed. The intercepted fragment before being fed into the CNN model, needs to be normalized as follows:

$$\bar{Q} = \frac{Q - \mu_Q}{\delta_Q} \tag{2}$$

where Q, $\bar{Q}$ are the discharging capacity data and normalized discharging capacity data, respectively. δ_Q and μ_Q are the training dataset' s standard deviation and mean value, respectively.

2.4. Empirical mode decomposition

Capacity degradation curves of LIBs are not exactly monotonically decreasing, because of some uncontrolled chemical reaction inside the battery. The capacity might recover at a small amount, which could be interpreted as capacity regeneration. This noise would disrupt the subsequent model to grasp the global capacity degradation trend seriously, so the predicted capacity degradation curve originating from the well-trained CNN model need to be decomposed to improve the accuracy of subsequent RUL prediction.

EMD algorithm was proposed by Huang et al. [31] to analyze nonlinear and non-stationary signals, which could transfer a group of time series into locally narrow band components, namely, intrinsic mode functions (IMFs). Compared with the other traditional method (wavelet decomposition and the wavelet packet decomposition), EMD is more suitable for processing nonlinear signals because the it does not need to select the decomposing parameters manually.

Through the process of EMD, the capacity degradation data $x(t)$ are decomposed into terms of IMFs and residual, representing the capacity regeneration noise of different frequencies and global capacity degradation trend, respectively. Then, the decomposition function could be represented as:

$$x(t) = \sum_{j=1}^{d} c_j(t) + r_d(t) \tag{3}$$

where $c_j(t)$ $(j = 1,2, \ldots, d)$ is the IMFs including different frequency bands ranging from high to low, reflecting the disruption of noise signals caused by capacity regeneration, $r_d(t)$ is the residual, representing the global capacity degradation trend, and d is the number of the modes.

The detailed decomposition of EMD is as follows:

(1) Confirm all the local extremum points (the local maxima and minima) of the time series $x(t)$.
(2) Fit the local maxima and minima to format the upper and lower envelope using the cubic spline interpolation function, denote the upper and lower envelope as $x_u(t)$ and $x_l(t)$, respectively.
(3) Compute the mean ($m(t)$) of the upper and lower envelops as follows:

$$m(t) = [x_l(t) + x_u(t)]/2 \tag{4}$$

(4) Compute a new data sequence $h(t)$ from $x(t)$ by subtracting $m(t)$, as shown as follows:

$$h(t) = x(t) - m(t) \tag{5}$$

(5) Judge whether the oscillating mode condition is satisfied. If yes, export the $x(t)$ as the residual $r_d(t)$, and stop the EMD computation. If not, go ahead to step (6).
(6) Regard $h(t)$ as one of the IMFs, namely, $c_j(t) = h(t)$.
(7) Replace $x(t)$ with the residual $r(t)$ as shown as follows:

$$r(t) = x(t) - c_j(t) \tag{6}$$

and then repeat the above.

It is worth noticing that the oscillating mode condition is defined by the equation below:

$$\sum_{t=1}^{M} \frac{\left[h_{j-1}(t) - h_j(t)\right]^2}{h_{j-1}^2(t)} \le \delta,\ j = 1, 2, \ldots, M \tag{7}$$

where M is the number of data points, representing the number of discharge curve in this case, and δ is the termination parameter, which is 0.05 in this study. When the iterative calculation result meets Eq. (7), the EMD calculation will be converged.

2.5. GRU unit

GRU unit, proposed by Cho et al. [32], chose a new type of hidden unit that has been motivated by the LSTM unit. Compared with LSTM, GRU combines the forget gate and the input gate into a single update gate and is also mixed with cellular state and hidden state. Hence, it has fewer parameters and a faster training speed. The structure of a GRU memory cell is shown in Fig. 3 below:

The output of a memory cell is controlled by the reset gate r_t and the update gate z_t, which are related to x_t and h_{t-1}. x_t and h_{t-1} denote the current input sequence and hidden state at the previous time point, respectively. These two kinds of gates have their respective missions. The r_t controls how much information in h_{t-1} could be ignored. The previously hidden state information is contained less when the value is smaller. The z_t is designed to control the impact of the previous information on the current moment. The larger the value is, the more

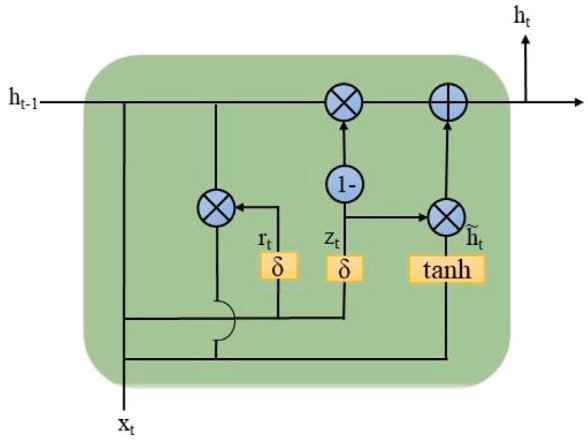

Fig. 3. Basic GRU structure.

previous information is brought in. The specific calculation process can be represented based on the following equations:

Reset gate:

$$r_t = \sigma(W_\tau \cdot [h_{t-1}, x_t]) \tag{8}$$

Update gate:

$$z_t = \sigma(W_z \cdot [h_{t-1}, x_t]) \tag{9}$$

Output:

$$\tilde{h}_t = \tanh\left(W \cdot [r_t * h_{t-1}, x_t]\right) \tag{10}$$

$$h_t = (1 - z_t) * h_{t-1} + z_t * \tilde{h}_t \tag{11}$$

2.6. GRU-FC model

In consideration of algorithmic complexity and accuracy comprehensively, a GRU-FC network structure, which is composed of 2 GRU layers and 2 FC layers, is constructed for LIBs RUL prediction in this study. Given the size of the open dataset about LIBs [33,34], the number of GRU is set to 40. A ReLU activation function is also placed between 2 FC layers and utilized to avoid potential vanishing gradient problems. The architecture of the GRU-FC model is illustrated in Fig. 4 with capacity prediction value as follows:

$$C(k)_{pred} = W_{12} \cdot [W_{h2} \cdot (W_{h1} \cdot h_t + b_1) + b_2] + b_3 \tag{12}$$

where $C(k)_{pred}$ is the predicted maximum discharging capacity at the k_{th} cycle, W is the weight matrix, and b is the bias matrix.

The Adam optimizer is also employed for parameter training in backpropagation to update weights. The batch size is set to 500. During the GRU-FC model training process, 70% of the training dataset was used to train the GRU-FC model. The remaining 30% of this data was randomly selected as a validation dataset to validate the training process. After training for 1000 epochs, the model with the lowest validation loss is picked up and used in the maximum discharging capacity prediction process. In order to avoid the overfitting problem in the training process of the GRU-FC model, the early stopping approach is also employed, and the patience is set to 10.

2.7. Data pre-processing method for GRU-FC model

The sliding window method is used in the GRU-FC model training and predicting process, as shown in Fig. 5. The residual of historical data with a length of $(n + 1)$ serves as the input and output of the GRU-FC model, in which the sequence from C_{t-n} to C_{t-1} ($[C_{t-n}, C_{t-n+1}, \cdots, C_{t-1}]$) is used as input and the last data C_t is the target data of this model. Meanwhile, the input data before being fed into the model, also need to be normalized as follows:

$$\bar{C} = \frac{C - \mu_C}{\delta_C} \tag{13}$$

where C, $\bar{C}$ are the maximum discharging capacity data and normalized maximum discharging capacity data, respectively. δ_C and μ_C are the training dataset' s standard deviation and mean value, respectively.

2.8. RUL prediction process

Algorithm 1 presents the overall process of RUL prediction, where Γ_{CNN} and Γ_{GRU-FC} represent the well-trained CNN model and GRU-FC model, respectively. F represents the discharging fragment. PC_b is the predicted capacity degradation curve before SP_{rul}, and Res is the PC_b's residual via EMD method. $INPUT_{GRU-FC}$ is the input of Γ_{GRU-FC} in which sliding window is applied to intercept data. When the end condition is met, the predicted capacity degradation curve after SP_{rul} (PC_a) could be gained, and $RUL_{prediction}$ is easily confirmed by comparing PC_a data with the failure threshold ($C_{failure}$). To decrease the computing cost and exhibit the degradation trajectory more clearly, only capacity data greater than 0.9 times $C_{failure}$ is predicted, and those less than $C_{failure}$ is not concerned.

3. Results and discussion

3.1. Experimental data

The performances of the proposed CEG approach are verified using two open battery datasets (CALCE-CX2 and CALCE-CS2) provided by the Center for Advanced Life Cycle Engineering [35], and the specifications and corresponding parameters of test batteries are shown in Table S2. The capacity degradation process of CALCE-CS2 is displayed in Fig. 6a, which are CS2-35, CS2-36, CS2-37, and CS2-38

Fig. 4. The network architecture of GRU-FC model.

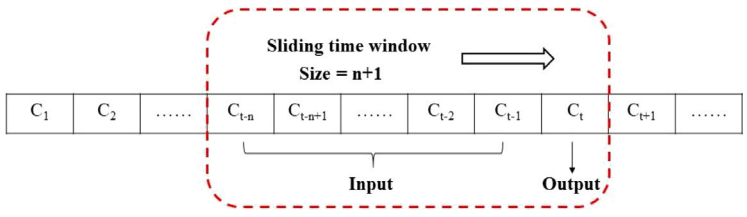

Fig. 5. The input and output data are based on a sliding window.

Algorithm 1 RUL prediction for test battery

Input: Every cycle's discharging fragment before SP_{rul}

Output: $RUL_{prediction}$

collect every cycle's discharging fragment before SP_{rul}:

$$F_1 = \left[\left[V_{s^1}, V_{s^1+1}, \cdots, V_{s^1+\alpha}\right], \left[Q_{s^1} - Q_{s^1-1}, Q_{s^1+1} - Q_{s^1-1}, \cdots, Q_{s^1+\alpha} - Q_{s^1-1}\right]\right]$$

$$F_2 = \left[\left[V_{s^2}, V_{s^2+1}, \cdots, V_{s^2+\alpha}\right], \left[Q_{s^2} - Q_{s^2-1}, Q_{s^2+1} - Q_{s^2-1}, \cdots, Q_{s^2+\alpha} - Q_{s^2-1}\right]\right]$$

$$\cdots$$

$$F_{SP_{rul}} = \left[\left[V_{s^{SP_{rul}}}, V_{s^{SP_{rul}}+1}, \cdots, V_{s^{SP_{rul}}+\alpha}\right], \left[Q_{s^{SP_{rul}}} - Q_{s^{SP_{rul}}-1}, Q_{s^{SP_{rul}}+1} - Q_{s^{SP_{rul}}-1}, \cdots, Q_{s^{SP_{rul}}+\alpha} - Q_{s^{SP_{rul}}-1}\right]\right];$$

normalize and then extrapolation:

$$C_1 = \Gamma_{CNN}(F_1)$$

$$C_2 = \Gamma_{CNN}(F_2)$$

$$\cdots$$

$$C_{SP_{rul}} = \Gamma_{CNN}(F_{SP_{rul}})$$

$$PC_b = \left[C_1, C_2, \cdots C_{SP_{rul}}\right]$$

decompose PC_b via EMD method:

$$\text{Res} = \left[\hat{C}_1, \hat{C}_2, \cdots, \hat{C}_{SP_{rul}}\right];$$

intercept Res data via sliding window:

$$INPUT_{GRU-FC} = \left[\hat{C}_{SP_{rul}-n+1}, \hat{C}_{SP_{rul}-n+2}, \cdots, \hat{C}_{SP_{rul}}\right];$$

set initial k=1 & **repeat**;

normalize and then extrapolation:

$$\hat{C}_{SP_{rul}+k} = \Gamma_{GRU-FC}\left(INPUT_{GRU-FC}\right);$$

update $INPUT_{GRU-FC}$:

$$INPUT_{GRU-FC} = \left[\hat{C}_{SP_{rul}+k-n+1}, \hat{C}_{SP_{rul}+k-n+2}, \cdots, \hat{C}_{SP_{rul}+k}\right];$$

cycle time: $k+=1$;

until the end condition $\hat{C}_{SP_{rul}+k} \le 0.9 \times C_{\text{failure}}$ is met:

$$PC_a = \left[\hat{C}_{SP_{rul}+1}, \hat{C}_{SP_{rul}+2}, \cdots, \hat{C}_{SP_{rul}+k}\right];$$

search the last capacity point meeting $\hat{C}_{SP_{rul}+k'} \ge C_{\text{failure}}$, and k' is $RUL_{\text{prediction}}$.

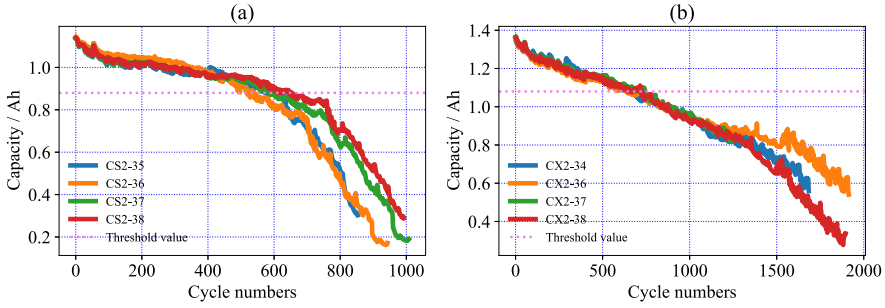

Fig. 6. Battery capacity degradation curves: (a) CALCE-CS2; (b) CALCE-CX2.

LIBs, respectively. The battery with 1.10 Ah was tested at a standard constant current/voltage protocol with a current rate of 0.5 C until the voltage reached 4.2 V, and then 4.2 V was sustained until the charging current dropped to below 0.05 A. For CALCE-CS2 dataset, their rated capacity is considered to be 1.10 Ah, and the failure threshold of RUL prediction is set to 0.88 Ah (80% of capacity rating). Fig. S1 displays the constant current discharging curves for CALCE-CS2. Because some batteries could not reach the *UVL* or *LVL*, the discretized discharging curve is restructured via a linear interpolation method with 10 mV intervals. The upper or lower voltage of the new discharging curve could be fixed at 4.181 V and 2.710 V, respectively. Therefore, the processing entire discharging curve contains 148 elements, meanwhile, capacity variation out of this voltage range could be ignored. The training dataset of CALCE-CS2 consists of three batteries (CS2-36, CS2-37, and CS2-38), and the remaining battery (CS2-35) serves as the testing dataset.

As shown in Fig. 6b, another dataset of CALCE-CX2 includes CX2-34, CX2-36, CX2-37, and CX2-38, exhibiting a more apparent linear degradation phenomenon than CALCE-CS2 due to different jellyroll configurations. Except for the higher capacity (1.35 Ah), the charging and discharging policies of CALCE-CX2 are similar to those of CALCE-CS2. For CALCE-CX2 batteries, their rated capacity is considered to be 1.35 Ah, and the failure threshold of RUL prediction is set to 1.08 Ah (80% of capacity rating). Fig. S2 displays the constant current discharging curves for CALCE-CX2. The linear interpolation method is also utilized to restructure the new discharging curve of CALCE-CX2. The upper or lower voltage of the new discharging curve could be fixed at 4.040 V and 2.700 V. Therefore, the processing entire discharging curve contains 134 elements. Meanwhile, the only first one thousand charging/discharging cycle data would be studied because the remaining data is far below its failure threshold. The training dataset

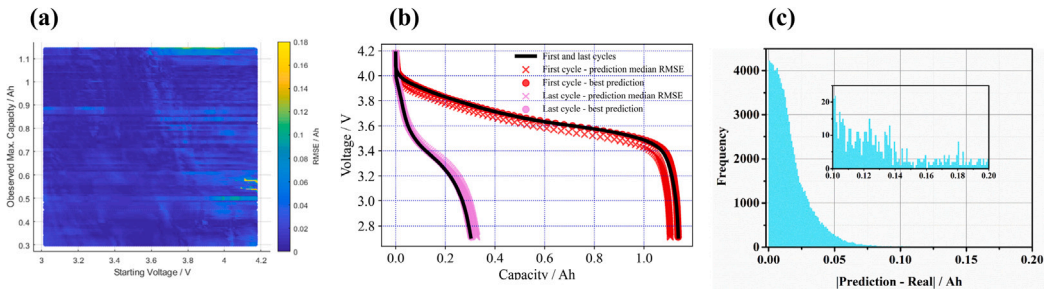

Fig. 7. Curve restructured results via CNN model (a) $RMSE_{CNN}$ of discharging-curve prediction for the CS2-35. (b) Examples of the curve estimation results at the first and last cycles of CS2-35. (c) The error distribution between real maximum discharging capacity and the corresponding values for CS2-35 battery.

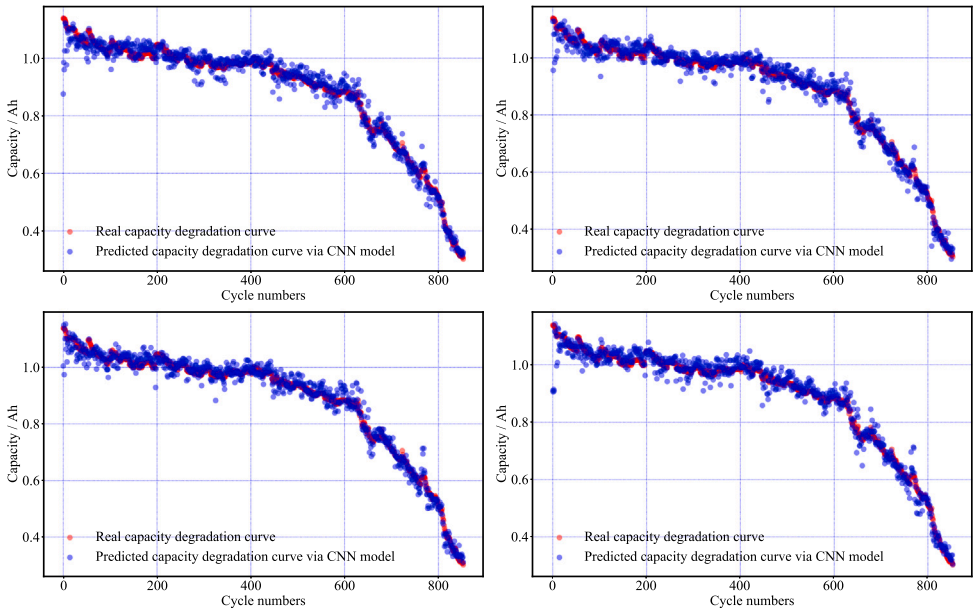

Fig. 8. Random 4 predicted all-cycle capacity degradation curves of CS2-35 battery via a well-trained CNN model, in which the predicted maximum discharging capacity of every cycle is based on the randomly picked discharging fragment.

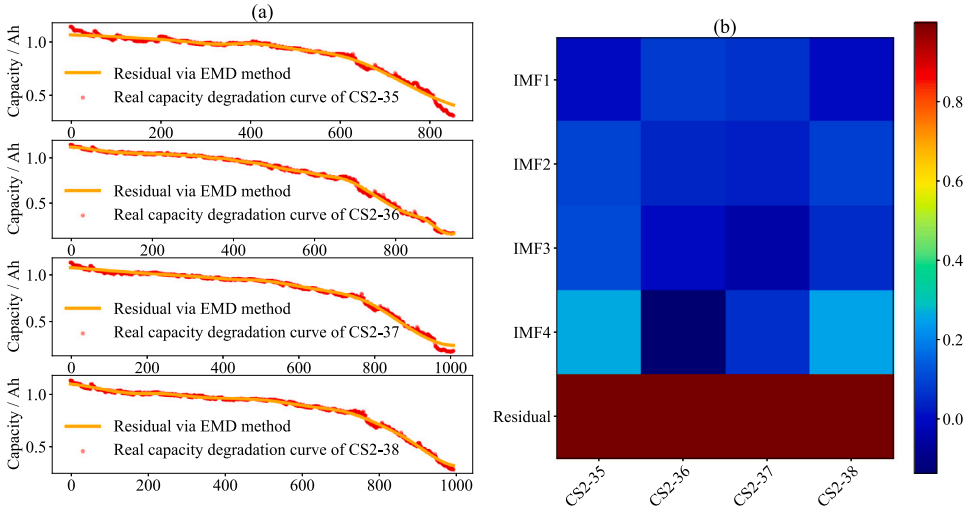

Fig. 9. (a) Residuals of CALCE-CS2 after EMD processing; (b) Pearson correlation coefficients between original curves with IMFs and residuals, respectively.

of CALCE-CX2 consists of three batteries (CX2-34, CX2-36, and CX2-37), and the remaining battery (CX2-38) serves as the test dataset. Additionally, there are a lot of noise signals caused by capacity regeneration in all capacity degradation curves, which would disturb the RUL prediction. In this study, the CALCE-CS2 dataset is utilized to testify the predicted performances of this proposed approach first, and the CALCE-CX2 dataset is utilized subsequently to testify the generalization ability of this approach.

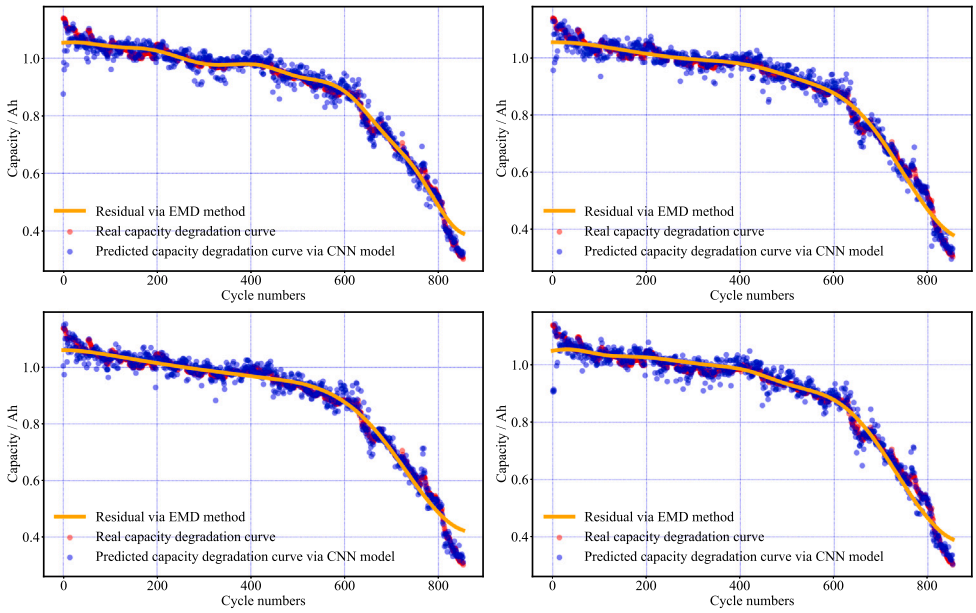

Fig. 10. Comparing the real capacity degradation curve of CS2-35 battery and residuals of the random 4 predicted all-cycle capacity degradation curves via the well-trained CNN model, in which the predicted maximum discharging capacity of every cycle is based on the randomly picked discharging fragment.

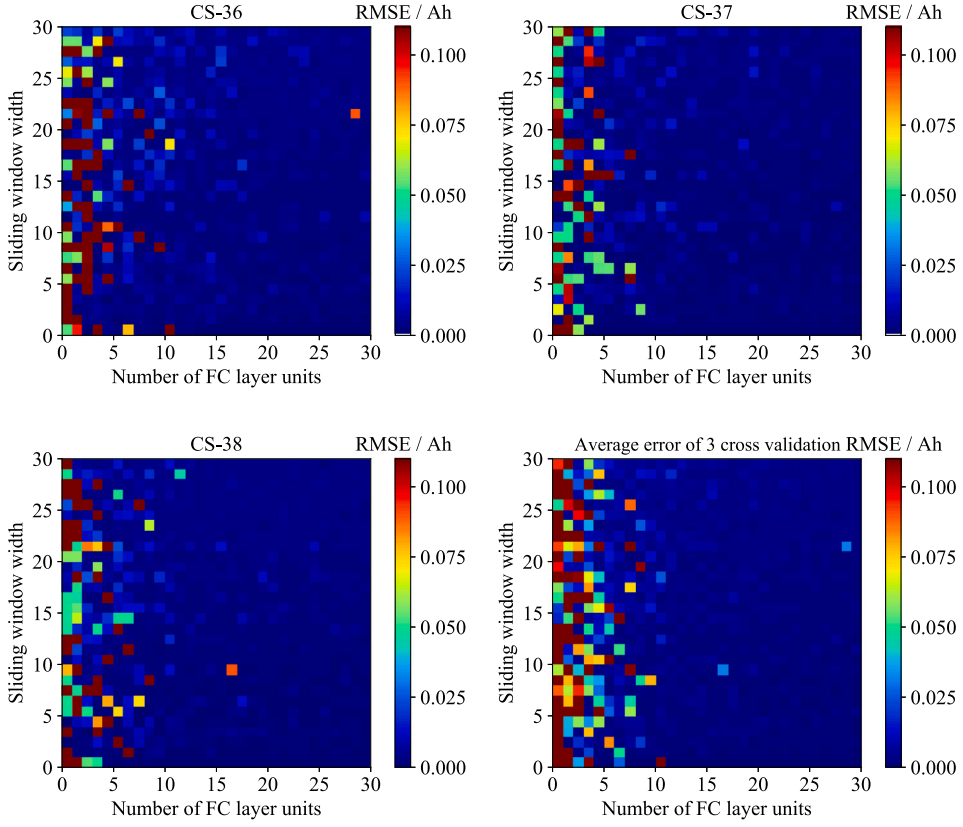

Fig. 11. Validation test of the GRU-FC model with the different number of FC neurons and the sliding window length based on the residuals of CS-36, CS-37, and CS-38 data.

3.2. Evaluation criteria

To evaluate the performances of the restructuring discharging curve and predicted maximum discharging capacity via the CNN model, the root mean square errors ($RMSE_{CNN}$) and absolute error ($AE_{Capacity}$) are employed, and the equations are as follows:

$$\mathrm{RMSE_{CNN}} = \sqrt{\frac{1}{n_1}\sum_{i=1}^{n_1}\left(\hat{Q}_i - Q_i\right)^2} \tag{14}$$

$$AE_{Capacity} = \left|\mathrm{Capacity_{prediction}} - \mathrm{Capacity_{true}}\right| \tag{15}$$

where n_1 is the element number of this discharging curve; Q_i and $\hat{Q}_i$ are the measured capacity and corresponding predicting value at the i^{th} point of this discharging curve, respectively; $Capacity_{prediction}$ and $Capacity_{true}$ are the predicting maximum discharging capacity and corresponding true value, respectively. The smaller values of these criteria represent higher prediction accuracy for the CNN model.

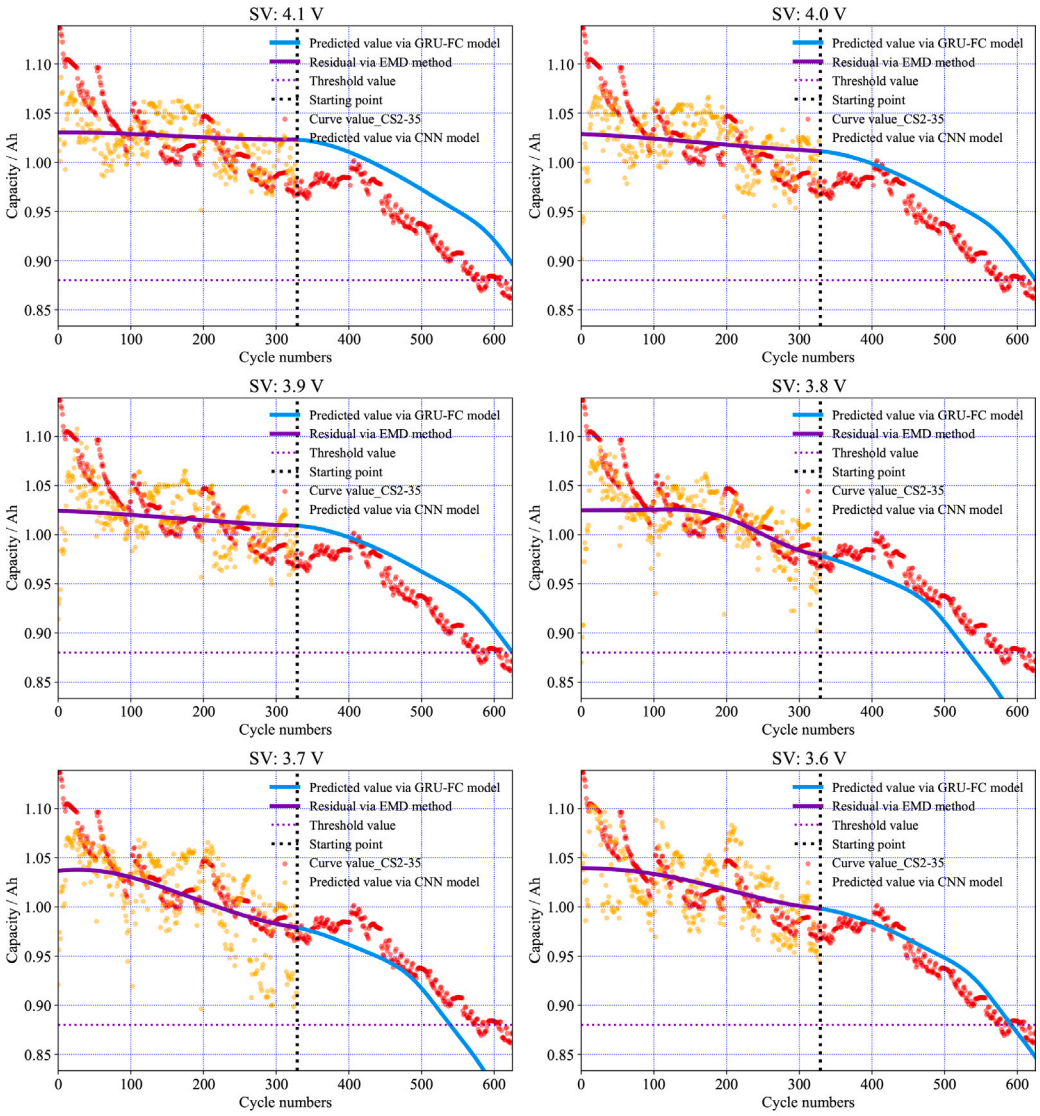

(a) SV from 4.1 V to 3.6 V

Fig. 12. RUL prediction of CEG approach for CS2-35 battery, when the fragment's SV of every cycle is set to fixed values.

To quantitatively evaluate the RUL prediction performances of the whole hybrid approach, absolute error (AE_{rul}), relative error (RE), and root mean square error ($RMSE_{rul}$) are used for evaluation, and they are shown as follows:

$$\mathrm{AE_{RUL}} = \left|\mathrm{RUL_{prediction}} - \mathrm{RUL_{true}}\right| \tag{16}$$

$$\mathrm{RE} = \frac{\left|\mathrm{RUL_{prediction}} - \mathrm{RUL_{true}}\right|}{\mathrm{RUL_{true}}} \times 100\% \tag{17}$$

$$RMSE_{rul} = \sqrt{\frac{1}{n_2}\sum_{k=1}^{n_2}\left(\hat{C}_k - C_k\right)^2} \tag{18}$$

where $RUL_{\mathrm{prediction}}$ denotes the predicted value of RUL, and RUL_{true} indicates the real value of RUL; n_2 is the number of predicted lengths between SP_{rul} and failure threshold; C_k is the real maximum discharging capacity value at the k^{th} cycle, and $\hat{C}_k$ is the corresponding predicted capacity values from GRU-FC model. The smaller values of the three criteria represent higher prediction accuracy for RUL prediction.

3.3. Predicted maximum discharging capacity based on the discharging fragment via CNN model

The restructured result of all discharging curves for CS2-35 are displayed in Fig. 7a, in which abscissa represents the starting voltage (SV) of the discharging fragments, and the ordinate represents the observed maximum discharging capacity corresponding to sampled discharging curve, namely, the recording discharging capacity at 2.710 V in raw data. For all battery lifetime, the well-trained CNN model can reconstruct the entire discharging curve with the average $RMSE_{CNN}$ of 11.2 mAh (1.02% of the nominal capacity of 1.10 Ah). Besides, as shown in Table 1, the $RMSE_{CNN}$ (7.8 mAh) values of low SV (3.01 ~ 3.60 V) are lower than those ($RMSE_{CNN}$: 14.6 mAh) of high SV (3.60 ~ 4.18 V). Namely, the restructured performances of the discharging curve could be guaranteed well when the input sequence starts at low voltage, which implies this voltage region processes more effective information [29]. The restructured results of the first and last discharging curve of CS2-35 are displayed in Fig. 7b. In this study, it is vital for the subsequent model to provide accurate every cycle's maximum discharging capacity as input. Fig. 7c exhibits the difference values between the real maximum discharging capacity and

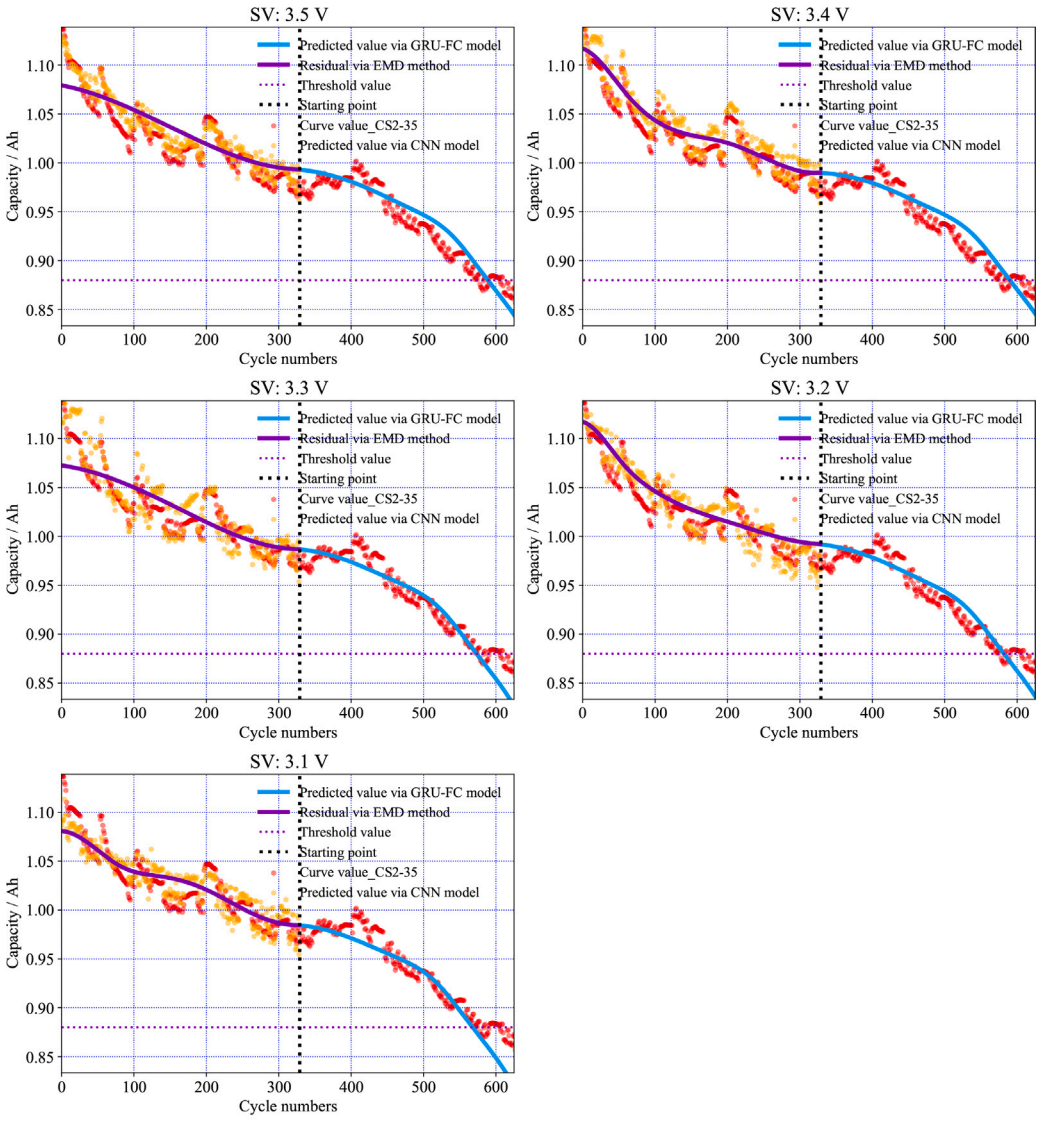

(b) *SV* from 3.5 V to 3.1 V

Fig. 12. (*continued*).

Table 1
Prediction errors of the CNN model for the CS2-35 battery.

SV of the discharging fragments /V	Average $RMSE_{CNN}$ /mAh	Average $AE_{Capacity}$ /mAh
3.01~4.18	11.2	17.9
3.01~3.60	7.8	11.4
3.60~4.18	14.6	24.4

the corresponding predicted value from the restructured discharging curve. It can be seen that these errors are centralized mainly near 0, implying the predicted results from the well-trained CNN model could agree well with the real discharging capacity. Meanwhile, as shown in Table 1, the average $AE_{Capacity}$ (11.4 mAh) values of low *SV* (3.01 ~ 3.60 V) are lower than those (average $AE_{Capacity}$: 24.4 mAh) of high *SV* (3.60 ~ 4.18 V), so the discharging fragment's *SV* could try to choose the region near the *LVL* to gain more precise maximum discharging capacity.

To demonstrate the potential of the predicted outcomes from the CNN model as the subsequent model input, Fig. 8 displays the random 4 predicted all-cycle capacity degradation curves of CS2-35 battery via a well-trained CNN model, in which the predicted maximum discharging capacity of every cycle is based on the randomly picked discharging fragment. It can be seen that the global trends of the predicted all-cycle capacity degradation curves are consistent with ground truth, so the well-trained CNN model could provide reliable input for the subsequent RUL prediction.

3.4. Decomposition results for capacity degradation curve by EMD method

During the capacity degradation process of LIBs, the capacity regeneration would produce an appreciable amount of noise to disrupt the RUL prediction. Hence, in this study, the EMD method is employed to extract the global trend of the training dataset's capacity degradation curves to serve as the training dataset for the GRU-FC model. Fig. 9a displays the original capacity degradation curves of the CALCE-CS2 batteries and the corresponding decomposed residuals via the EMD method. It can be seen that the extracted residual curve is smooth and highly coincident with the trend of the original curve, which implies that the EMD method could obtain the main characteristics of the capacity degradation curve and eliminate the influences of capacity regeneration noise. Fig. 9b displays the Pearson correlation coefficients between original curves with IMFs and residuals, respectively. It is

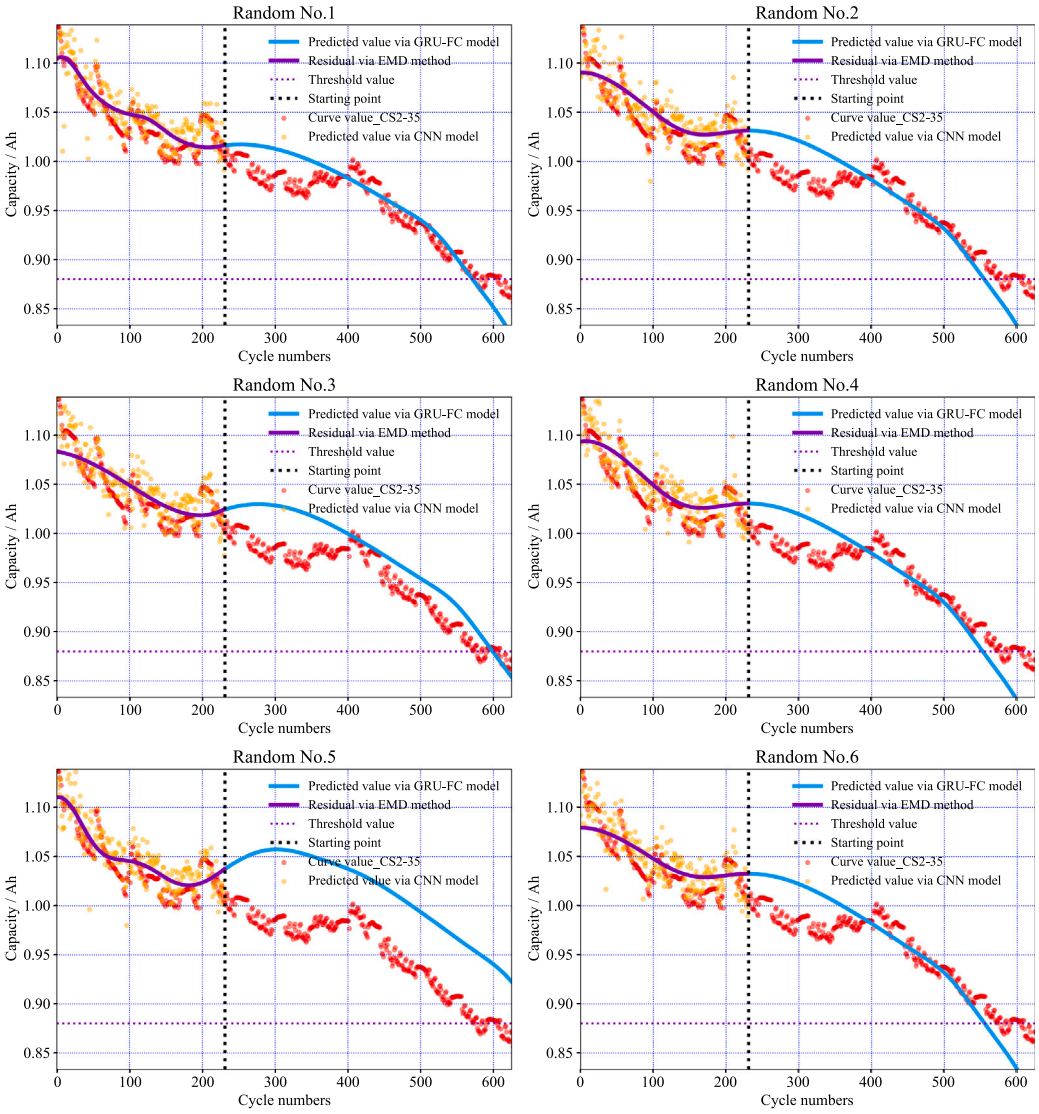

Fig. 13. RUL prediction of CEG approach for CS2-35 battery when the fragment's SV is randomly selected from 3.60 V to 3.01 V, for every discharging curve before SP_{rul} (231 cycles; ~40% of the degradation data) is chosen randomly.

clear that the correlation coefficients between all the residual and their original data are infinitely close to 1, and those of the other IMFs are overshadowed by contrast, demonstrating that the residuals are highly relevant to the original data. In order to exhibit how the EMD method could avoid the disruption of capacity regeneration, the fast Fourier transformer approach is employed to study the relationship between frequency and amplitude. As shown in Fig. S3, a case study of the CS2-35 battery is conducted. The amplitude of the high-frequency IMF is lower than that of low-frequency IMF, and there is no obvious frequency for residual, indicating that the extracted residual almost certainly contained no noise signal caused by capacity regeneration. Therefore, the EMD method can avoid the disruption of capacity regeneration, and extract the trend of the capacity degradation curve, efficiently.

Besides, as shown in Fig. 8, there is still non-negligible capacity regeneration for the predicted capacity degradation curve from the CNN model. Therefore, the denoising processing also could be carried out for the predicted outcome from the CNN model for the subsequent accurate RUL prediction. Meanwhile, the accuracy of RUL prediction might not be improved even if all the IMFs are predicted by other arithmetic and added to the final results [36]. This is because there is a relatively high gap between the IMFs of the real capacity degradation curve and those of the predicted capacity degradation curve from the CNN model, and the extra calculation also would generate additional cost. To exhibit the decomposition performances of the predicted outcomes from the CNN model, Fig. 10 displays the decomposition results of the predicted all-cycle capacity degradation curve of the CS2-35 battery via the well-trained CNN model, in which the predicted maximum discharging capacity of every cycle originated from the randomly picked discharging fragment. It is clear that the decomposed residual curves also could reflect the main trend of the real capacity degradation curve, implying the denoising efficiency of the EMD method. Therefore, before SP_{rul}, the residual of the predicted capacity degradation curve from CNN model could serve as the input for the well-trained GRU-FC model, which decreases the disruption of capacity regeneration.

3.5. Hyperparametric optimization of the GRU-FC model on training dataset

The number of FC neurons and the sliding window length are vital for the performance of GRU-FC model, so the grid search and three-fold cross-validation are employed for hyperparametric optimization. Fig. 11 shows the grid-search results of the GRU-FC model with the variational combination of FC neurons and the sliding window length based on the residuals of CS-36, CS-37, and CS-38 data. When the

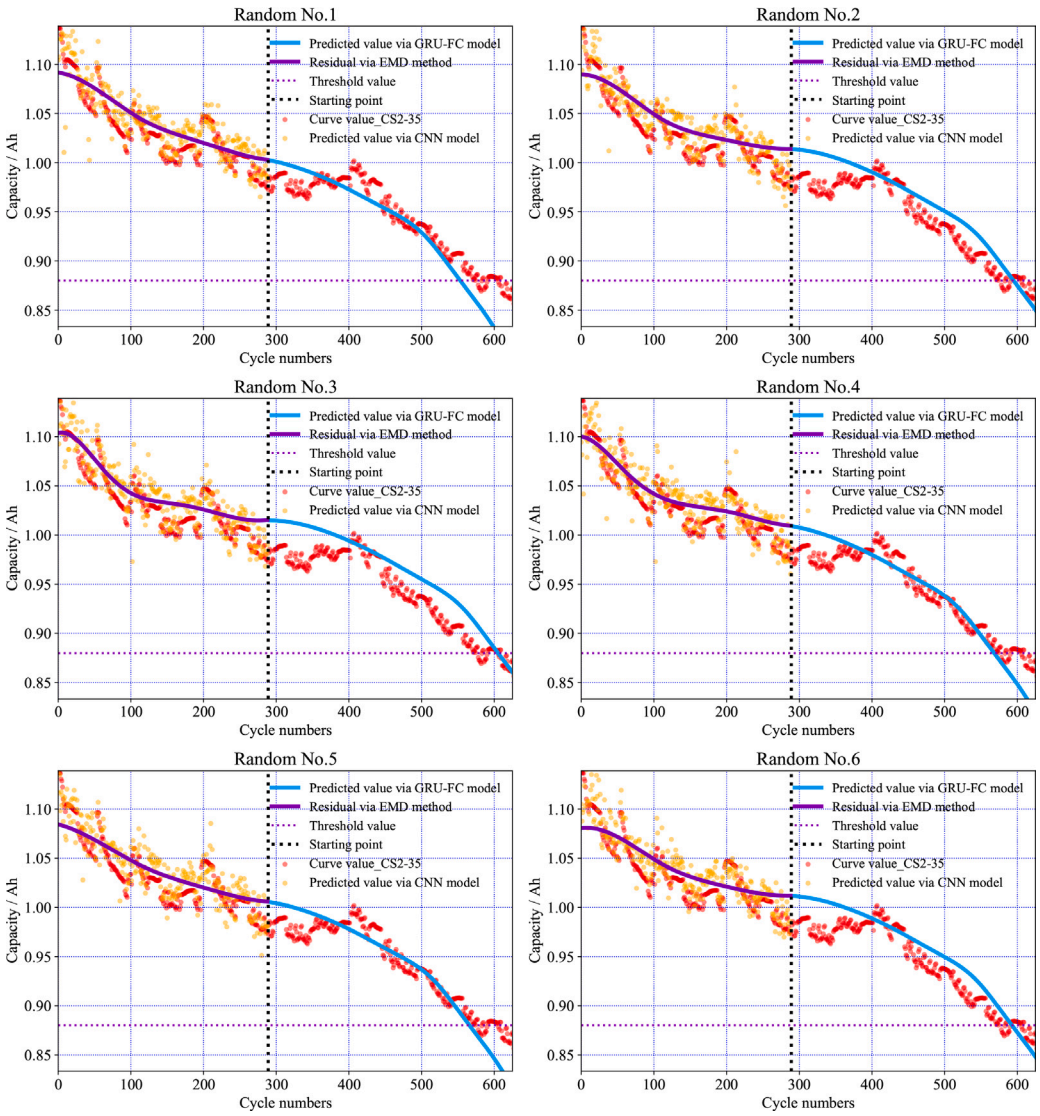

Fig. 14. RUL prediction of CEG approach for CS2-35 battery when the fragment's *SV* is randomly selected from 3.60 V to 3.01 V, for every discharging curve before SP_{rul} (289 cycles; ~50% of the degradation data) is chosen randomly.

FC neuron units are between 17 and 28, and the sliding window length is between 10 and 21, the $RMSE_{rul}$ error could reach the minimum value. In order to decrease the model complexity, the number of FC neurons and the sliding window length are set to 20 and 20, respectively. The detailed structure data of GRU-FC model are listed in Table S3.

3.6. Degradation trajectory and RUL prediction results of test dataset after SP_{rul}

According to the results of 3.3, the intercepted discharging fragment's *SV* play a great role in the predicted maximum discharging capacity, so the influence of the fragment's *SV* on RUL prediction would be investigated. Firstly, before SP_{rul}, discharging fragment with the same *SV* is intercepted in every cycle. Then, those fragments serve as the input of a well-trained CNN model to gain the predicted maximum discharging capacity, which combines to form the predicted capacity degradation curve before SP_{rul}. After EMD decomposition, the residual of this predicted curve from the CNN model serves as the input of the well-trained GRU-FC model. Figs. 12a and 12b show the RUL prediction result when the fragment's *SV* of every cycle is set to fixed values. When the fragment's *SV* gets closer to 3.1 V (near *LVL*), the residual (violet full line) decomposed from the predicted maximum discharging capacity from the CNN model (orange points), matches well with the global trend of real capacity degradation (red points before SP_{rul}). Meanwhile, the predicted capacity degradation trajectory from the GRU-FC model (light blue full line) matches well with the real capacity degradation trajectory (red points after SP_{rul}). This result is consistent with the above restructured results of the discharging curve, namely, the closer the fragment's *SV* gets to *LVL*, the higher prediction accuracy it is. When the more accurate predicted capacity degradation data from CNN model serves as the subsequent model input for RUL prediction, the degradation trend of the test battery could be well acquired by the well-trained GRU-FC model with learned characteristics from the source domain. As shown in Table 2, the RUL prediction errors (*RE*: 1.0381%; AE_{rul}: 6 cycles at 3.1 V) near *LVL* are remarkably lower than those errors (*RE*: 12.2837%; AE_{rul}: 71 cycles at 4.1 V) near *UVL*. Besides, when the discharging fragment's *SV* is less than 3.7 V, the prediction errors would decrease notably, which agree well with the results of predicting capacity degradation trajectory. Therefore, it can also be concluded that the discharging fragments' *SV* should be set to near *LVL* as far as possible if in practice.

Based on the above discussion, when the fragment's *SV* of every discharging curve is picked up near *LVL*, the more accurate RUL prediction

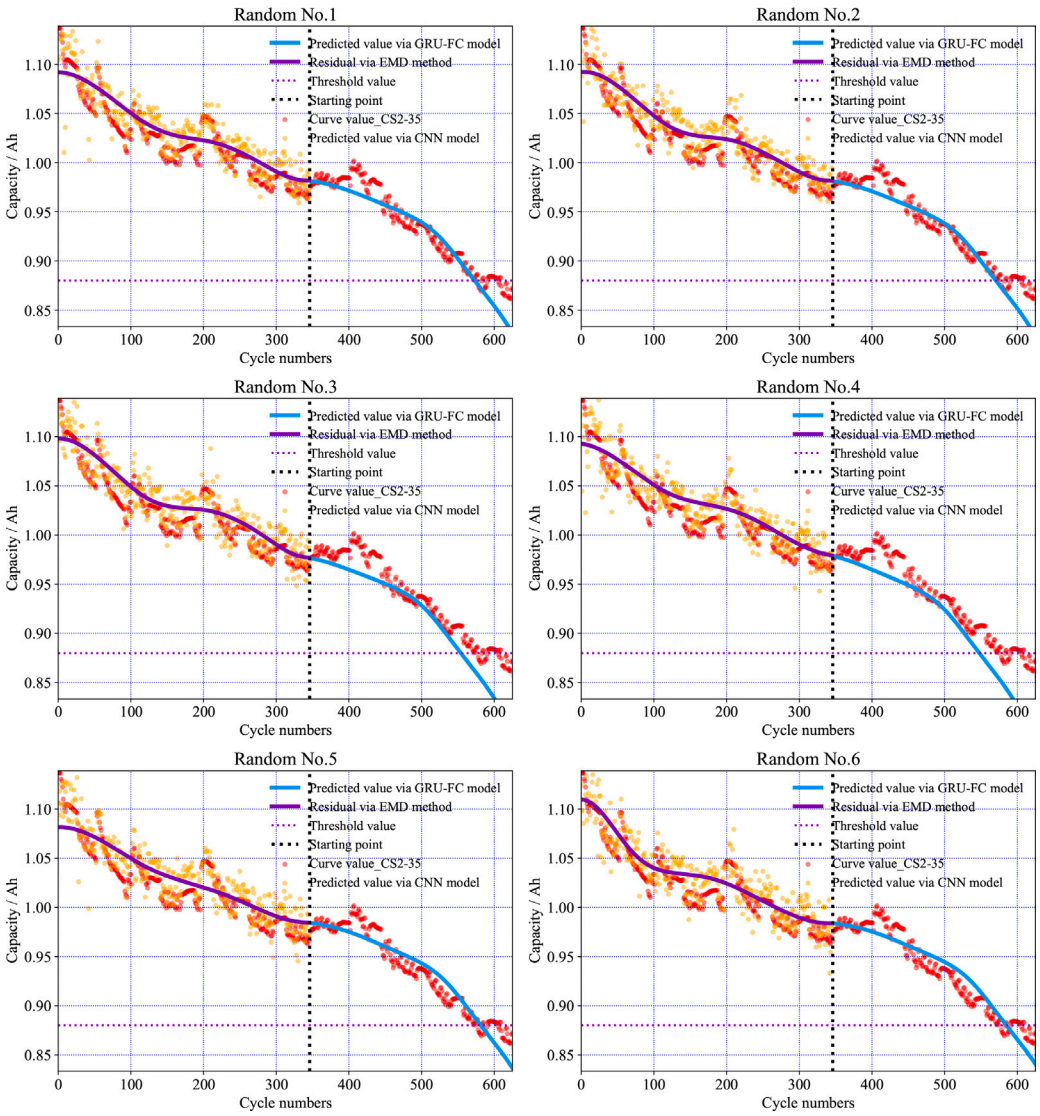

Fig. 15. RUL prediction of CEG approach for CS2-35 battery when the fragment's SV is randomly selected from 3.60 V to 3.01 V, for every discharging curve before SP_{rul} (346 cycles; ~60% of the degradation data) is chosen randomly.

Table 2
Prediction errors of CEG approach for the CS2-35 battery, when the fragment's SV of every cycle is set at fixed values.

SV/V	RE/%	$RUL_{prediction}$/cycles	AE_{rul}/cycles	$RMSE_{rul}$/Ah
4.1	12.2837	649	71	0.0414
4.0	9.3426	632	54	0.0139
3.9	9.3426	632	54	0.0311
3.8	7.2664	536	42	0.0247
3.7	6.0554	543	35	0.0209
3.6	3.2872	597	19	0.0174
3.5	2.7682	594	16	0.0156
3.4	2.9412	595	17	0.0154
3.3	0.0000	578	0	0.0117
3.2	1.3841	586	8	0.0135
3.1	1.0381	572	6	0.0116

could still be realized, so the fragment's SV could randomly selected within a specific range (from 3.60 V to 3.01 V for CS2-35). Figs. 13 and 14, and 15 display the RUL prediction result when the discharging fragment's SV is randomly selected from 3.60 V to 3.01 V, for every discharging curve before SP_{rul}. Whether the SP_{rul} is ~40% (231 cycles), ~50% (289 cycles), or ~60% (343 cycles) of the entire degradation data, the predicted capacity degradation trajectory from the GRU-FC model (light blue full line) is close to the real capacity degradation trajectory (red points after SP_{rul}), even when discharging fragments are picked up randomly within a specific voltage range. Based on the well-trained CNN model and EMD method, the discomposed residual reflects the global trend of the capacity degradation curve before SP_{rul}. Then, the well-trained GRU-FC model could rapidly and accurately predict test batterie's properties, based on the previous common characteristics of training dataset. As shown in Table 3, when the SP_{rul} is 346 cycles, the $RMSE_{rul}$ (the range: 0.0114 ~ 0.0189 Ah; the mean value: 0.0136 Ah), RE (the range: 0.6920% ~ 5.1903%, the mean value: 2.1915%) and AE_{rul} values (the range: 4 ~ 30 cycles, the mean value: 12 cycles),

Table 3
Prediction errors of the CEG approach for the CS2-35 battery when the fragment's SV is randomly selected from 3.60 V to 3.01 V, for every discharging curve before SP_{rul} (231, 289, and 346 cycles).

SP_{rul}	Random no.	RE/%	$RUL_{prediction}$ /cycles	AE_{rul} /cycles	$RMSE_{rul}$ /Ah
231 cycles (~40% of the entire degradation data)	1	1.0381	572	6	0.0189
	2	3.9792	555	23	0.0240
	3	3.6332	599	21	0.0315
	4	4.3253	553	25	0.0236
	5	15.5709	668	90	0.0639
	6	3.8062	556	22	0.0244
289 cycles (~50% of the entire degradation data)	1	4.1522	554	24	0.0156
	2	2.9412	595	17	0.0225
	3	4.8443	606	28	0.0262
	4	1.7301	568	10	0.0155
	5	2.0761	566	12	0.0144
	6	2.5952	563	15	0.0211
346 cycles (~60% of the entire degradation data)	1	0.6920	574	4	0.0114
	2	1.2111	571	7	0.0115
	3	4.1522	554	24	0.0161
	4	5.1903	548	30	0.0181
	5	0.6920	582	4	0.0119
	6	1.2111	585	7	0.0128

are a little lower than the $RMSE_{rul}$ (the range: 0.0144 ~ 0.0262 Ah; the mean value: 0.0192 Ah), RE (the range: 1.7301% ~ 4.8443%, the mean value: 3.0565%) and AE_{rul} (the range: 10 ~ 28 cycles, the mean value: 18 cycles) when SP_{rul} is 289 cycles, and much lower the $RMSE_{rul}$ (the range: 0.0189 ~ 0.0639 Ah; the mean value: 0.0311 Ah), RE (the range: 1.0381% ~ 15.5709%, the mean value: 5.3922%) and AE_{rul} (the range: 6 ~ 90 cycles, the mean value: 31 cycles) when SP_{rul} is 231 cycle. This result could be ascribed to the increased accumulating errors along with rolling prediction. Therefore, it is vital for enhancing accuracy of RUL prediction to gain latest data timely, in practice.

3.7. Prediction performance of the CEG approach on CALCE-CX2 dataset

To investigate the general applicability of the CEG approach, the CALCE-CX2 dataset is also studied. Firstly, the CNN model is retrained because of the different discharging voltage ranges between CALCE-CS2 and CALCE-CX2. As shown in Fig. S4a and Table S4, the average $RMSE_{CNN}$ value of the restructured discharging curve is about 36.8 mAh (2.73% of the nominal capacity of 1.35 Ah for CX2-38), and the $RMSE_{CNN}$ (25.4 mAh) and $AE_{Capacity}$ (13.9 mAh) values of low SV (3.01 ~ 3.50 V) are still lower than those ($RMSE_{CNN}$: 48.2 mAh; $AE_{Capacity}$: 29.3 mAh) of high SV (3.50 ~ 4.00 V), which is same as the above result of the CS2-35 battery. The restructured results of the first and last discharging curve of CX2-38 are displayed in Fig. S4b. Meanwhile, Fig. S4c shows the error distribution between the predicted maximum discharging capacity and ground truth, which is also centralized mainly near 0, implying that the maximum discharging capacity could also be predicted accurately via the well-trained CNN model based on the CX2-38 battery's discharging fragments. Fig. S5 displays the difference between predicted values from the CNN model and ground truth. The global trends of the random 4 predicted all-cycle capacity degradation curves, agree well with the real degradation curve, implying the universality of the CNN model. Fig. S6 displays the decomposition results of the random 4 predicted all-cycle capacity degradation curves from the well-trained CNN model, in which the predicted maximum discharging capacity of every cycle originated from the randomly picked discharging fragment. The decomposed residual from the predicted all-cycles discharging capacity curve could also reflect the global trend of the real degradation curve. Therefore, for the CX2-38 battery, before SP_{rul}, the residual decomposed from the predicted capacity degradation curve could serve as the input for the well-trained GRU-FC model.

The capacity degradation of adjacent cycles between the CALCE-CX2 dataset and the CALCE-CS2 dataset are very similar, so the hyper-parameters of the GRU-FC model remain unchanged. After extracting the residual of the CALCE-CX2 training dataset, the GRU-FC model is also constructed and then trained. Meanwhile, based on the result of the restructured discharging curve about CX2-38, the fragment's SV is randomly selected within a specific range (3.50 V ~ 3.01 V), to guarantee the subsequent RUL prediction. Fig. 16 (SP_{rul} = 258 cycles (~40% of the degradation data)), Fig. 17 (SP_{rul} = 323 cycles (~50% of the degradation data)), and Fig. 18 (SP_{rul} = 387 cycles (~60% of the degradation data)) exhibit the RUL prediction result when the discharging fragment's SV of every cycle before SP_{rul} is randomly selected from 3.50 V to 3.01 V. The predicted degradation trajectory after SP_{rul} is consistent with the real curve, further indicating the feasibility and robustness of the CEG approach. Although the capacity degradation curves of the CALCE-CX2 dataset exhibit more linear changes than those of the CALCE-CS2 dataset, the RUL prediction accuracy ($RE \leq$ 7.0%) of the CALCE-CX2 dataset is higher than those ($RE \leq$ 5.4%) of CALCE-CS2 dataset, which could be assigned to the relatively low prediction accuracy of the maximum discharging capacity from the CNN model for the CX2-38 battery.

3.8. Comparison with other methods

Table 4 summarizes the comparison between the results obtained with the proposed method for the CALCE-CS2 dataset and the RUL prediction results available in the literature. It can be seen that the input data used in almost all other technologies cover the entire degradation data before SP_{rul} instead of the partial discharge data used in this work. The indicator RE is comparable among different methods even if they use different dataset. Despite the difference in the training amount of degradation data, the proposed approach can still achieve the results with tolerable prediction error compared with other methods which use almost the same SP_{rul}. Especially, the proposed approach is the only one that can make the prediction just requiring discharging fragments of ~20% capacity ratio range as input compared with the listed methods, which remarkably reduces the dependence on the data collection. Meanwhile, the input fragment's SV does not need to be fixed in the discharging process.

4. Conclusion

This work proposes a hybrid data-driven approach consisting of the CNN model, EMD method, and GRU-FC model, which realizes excellent LIBs RUL prediction with discharging fragments. The main innovations of this article are: (i) for the RUL prediction, the raw data is composed of the discharging fragments, which could reduce time cost and make

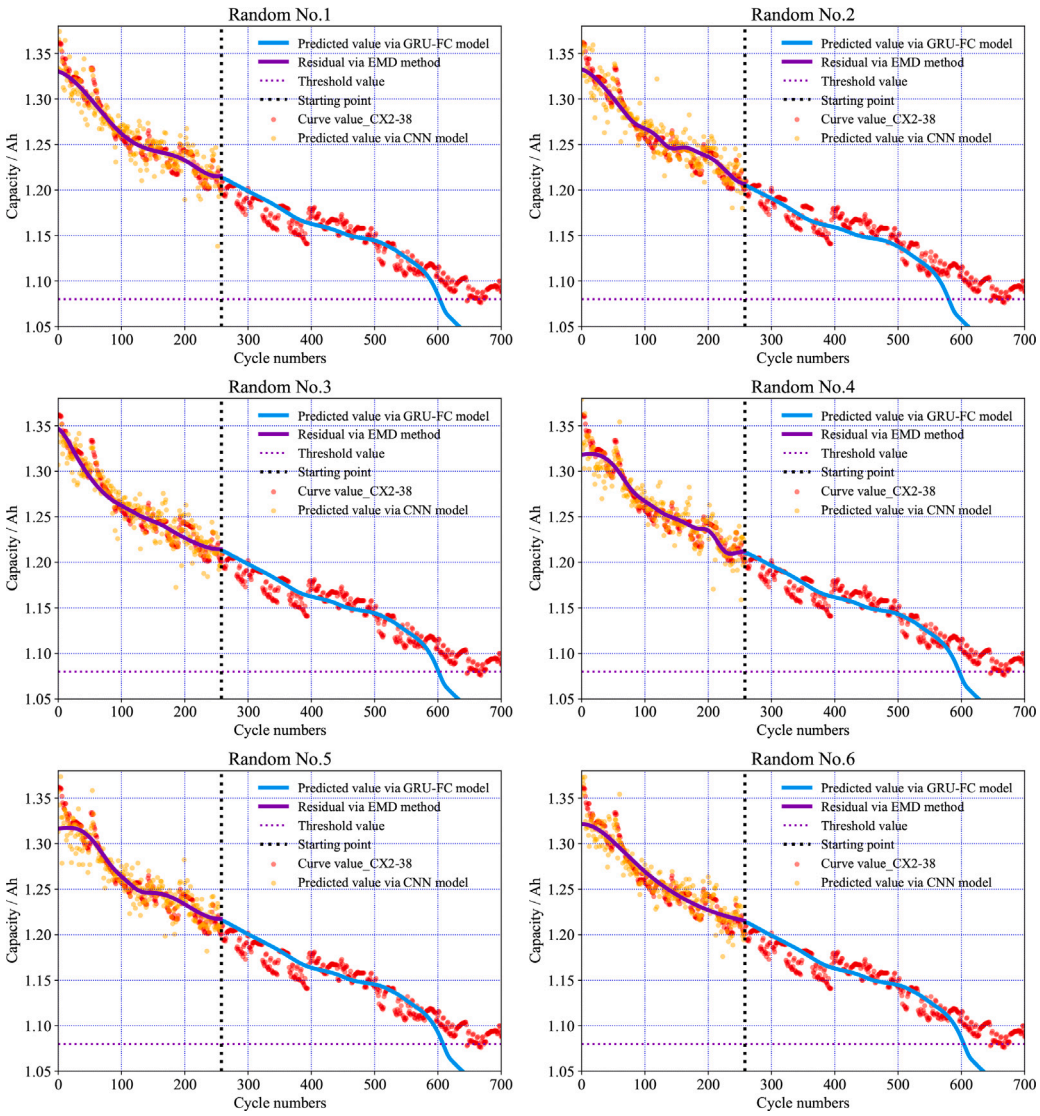

Fig. 16. RUL prediction of CEG approach for CX2-38 battery when the fragment's SV is randomly selected from 3.50 V to 3.01 V, for every discharging curve before SP_{rul} (258 cycles; ~40% of the degradation data) is chosen randomly.

Table 4
Comparison with other methods of RUL prediction results.

Methods	RE /%	$RMSE_{rul}$ /Ah	Requirements for input data
Proposed method	≤5.3922	≤0.0311	Discharging fragment of ~20% capacity ratio range from ~40% of the degradation data
	≤3.0565	≤0.0192	Discharging fragment of ~20% capacity ratio range from ~50% of the degradation data
	≤2.1915	≤0.0136	Discharging fragment of ~20% capacity ratio range from ~60% of the degradation data
TL-LSTM-PF[a] [37]	3.0	0.0110	~50% of the entire degradation data
DNN+IRes2Net-BiGRU-FC[b] [38]	8.7	0.0193	~43% of the entire degradation data
SDDL[c] [34]	0.86	0.0171	~50% of the entire degradation data
AR-RPF[d] [39]	14.06	-[f]	~36% of the entire degradation data
EMD-ARIMA[e] [40]	16.0	0.0209	~36% of the entire degradation data

[a] TL-LSTM-PF: the fusion method of LSTM based on transfer learning and particle filter model.
[b] DNN+Res2Net-Bidirectional Gated Recurrent Unit-Fully Connected.
[c] a sequence decomposition and deep learning.
[d] autoregressive model with autoregressive moving average.
[e] autoregressive integrated moving average model combining with EMD.
[f] the symbol "–" denotes "unavailable".

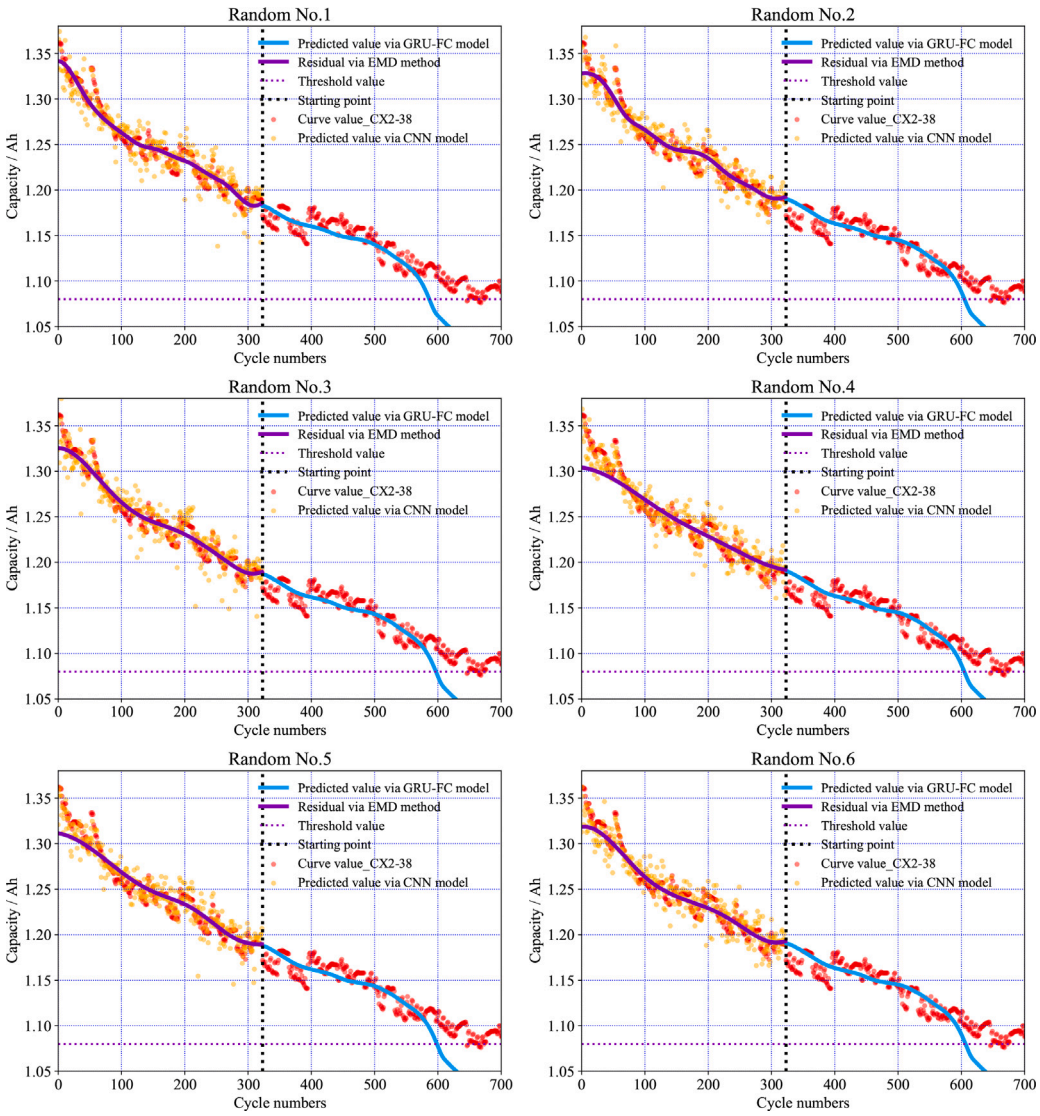

Fig. 17. RUL prediction of CEG approach for CX2-38 battery when the fragment's SV is randomly selected from 3.50 V to 3.01 V, for every discharging curve before SP_{rul} (323 cycles; ~50% of the degradation data) is chosen randomly.

it more suitable for the actual application; (ii) the well-trained CNN model could accurately predict the every cycle's maximum discharging capacity, and then the global degradation trend before SP_{rul} could be decomposed via EMD method. Finally, based on the decomposed residual, the well-trained GRU-FC model could estimate the capacity degradation trajectory after SP_{rul} because it already grasps this type battery's unique degradation characteristics; (iii) the proposed hybrid approach is tested on two open battery datasets, which exhibit less than 7.0% based on the discharging fragment of the ~20% capacity ratio range from 40% to 60% of the degradation data. Compared with other studies, the approach in this work performs significantly in terms of estimation accuracy and data requirements.

In the future, we will further explore the utilization of the approach in scenarios involving multiple charging/discharging protocols for batteries. Meanwhile, how to employ the pre-trained approach from one dataset to estimate the other dataset with different working condition is another major concern of our future research.

CRediT authorship contribution statement

Yunpeng Liu: Writing – original draft, Conceptualization. **Bo Hou:** Writing – review & editing. **Moin Ahmed:** Writing – review & editing. **Zhiyu Mao:** Writing – review & editing, Methodology, Investigation. **Jiangtao Feng:** Supervision. **Zhongwei Chen:** Supervision, Resources.

Declaration of competing interest

The authors declare that they have no known competing financial interests or personal relationships that could have appeared to influence the work reported in this paper.

Data availability

Data will be made available on request.

Acknowledgments

This work was supported by the National Natural Science Foundation of China (Grant No. 52102112), and the Fundamental Research Funds for the Central Universities, China (Grant No. xzy012022072). The data used in this article include: (1) data (https://calce.umd.edu/battery-data).

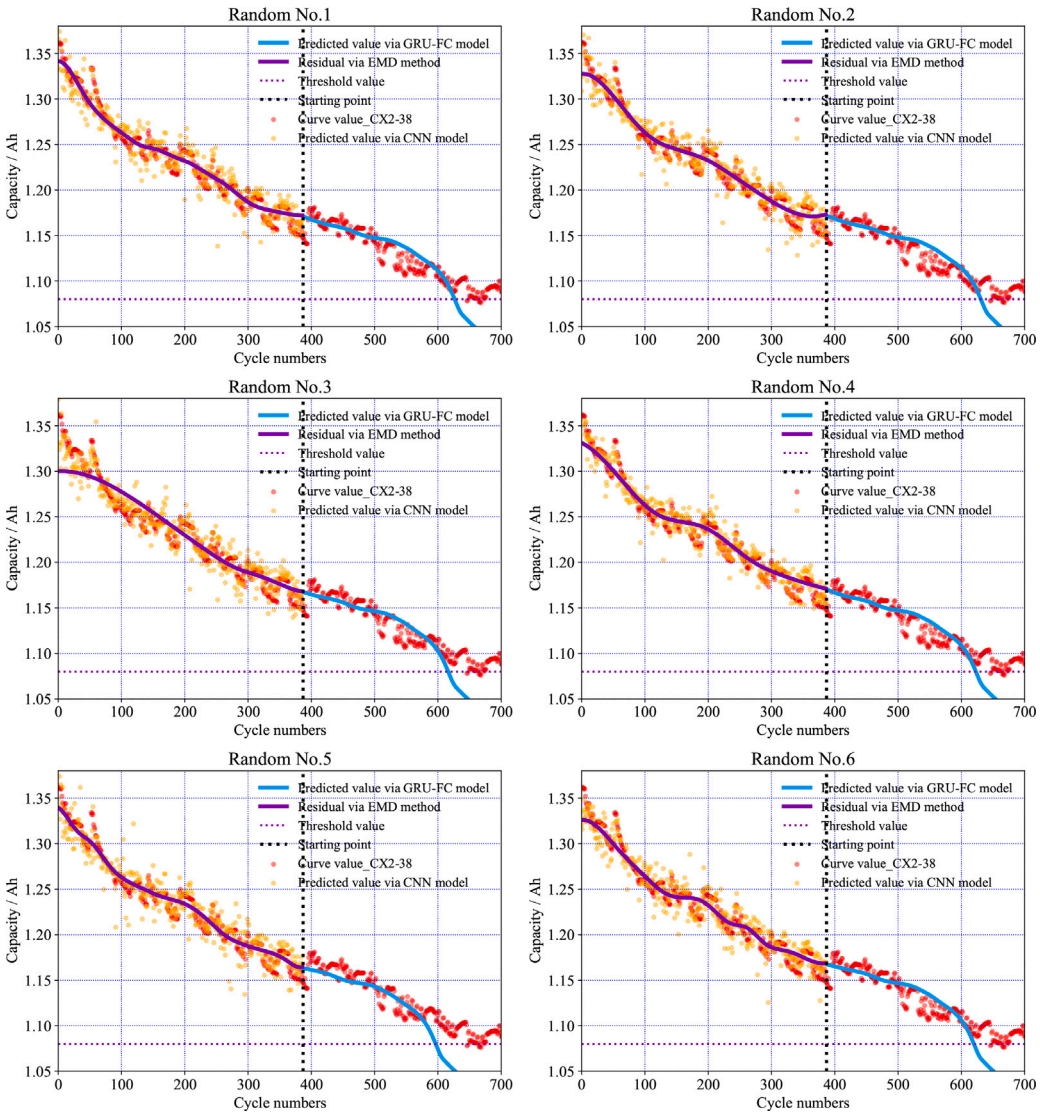

Fig. 18. RUL prediction of CEG approach for CX2-38 battery when the fragment's *SV* is randomly selected from 3.50 V to 3.01 V, for every discharging curve before SP_{rul} (387 cycles; ~60% of the degradation data) is chosen randomly.

Appendix A. Supplementary data

Supplementary material related to this article can be found online at https://doi.org/10.1016/j.apenergy.2023.122555.

References

[1] Severson KA, Attia PM, Jin N, Perkins N, Jiang B, Yang Z, et al. Data-driven prediction of battery cycle life before capacity degradation. Nat Energy 2019;4(5):383–91.

[2] Che Y, Deng Z, Li P, Tang X, Khosravinia K, Lin X, Hu X. State of health prognostics for series battery packs: A universal deep learning method. Energy 2022;238:121857.

[3] Tian J, Xiong R, Shen W, Lu J. State-of-charge estimation of LiFePO4 batteries in electric vehicles: A deep-learning enabled approach. Appl Energy 2021;291:116812.

[4] Zhang Y, Tang Q, Zhang Y, Wang J, Stimming U, Lee AA. Identifying degradation patterns of lithium ion batteries from impedance spectroscopy using machine learning. Nature Commun 2020;11(1):1706.

[5] Fei Z, Zhang Z, Yang F, Tsui K-L. A deep attention-assisted and memory-augmented temporal convolutional network based model for rapid lithium-ion battery remaining useful life predictions with limited data. J Energy Storage 2023;62:106903.

[6] Huang Y, Tang Y, VanZwieten J. Prognostics with variational autoencoder by generative adversarial learning. IEEE Trans Ind Electron 2021;69(1):856–67.

[7] Hsu C-W, Xiong R, Chen N-Y, Li J, Tsou N-T. Deep neural network battery life and voltage prediction by using data of one cycle only. Appl Energy 2022;306:118134.

[8] Lei Y, Li N, Gontarz S, Lin J, Radkowski S, Dybala J. A model-based method for remaining useful life prediction of machinery. IEEE Trans Reliab 2016;65(3):1314–26.

[9] Downey A, Lui Y-H, Hu C, Laflamme S, Hu S. Physics-based prognostics of lithium-ion battery using non-linear least squares with dynamic bounds. Reliab Eng Syst Saf 2019;182:1–12.

[10] Le Son K, Fouladirad M, Barros A, Levrat E, Iung B. Remaining useful life estimation based on stochastic deterioration models: A comparative study. Reliab Eng Syst Saf 2013;112:165–75.

[11] Yan W, Zhang B, Zhao G, Tang S, Niu G, Wang X. A battery management system with a lebesgue-sampling-based extended Kalman filter. IEEE Trans Ind Electron 2019;66(4):3227–36.

[12] Lipu MH, Hannan M, Hussain A, Hoque M, Ker PJ, Saad MM, et al. A review of state of health and remaining useful life estimation methods for lithium-ion battery in electric vehicles: Challenges and recommendations. J Cleaner Prod 2018;205:115–33.

[13] Li X, Yuan C, Wang Z. State of health estimation for li-ion battery via partial incremental capacity analysis based on support vector regression. Energy 2020;203:117852.

[14] Li X, Yuan C, Li X, Wang Z. State of health estimation for li-ion battery using incremental capacity analysis and Gaussian process regression. Energy 2020;190:116467.

[15] Yuchen S, Datong L, Yandong H, Jinxiang Y, Yu P. Satellite lithium-ion battery remaining useful life estimation with an iterative updated RVM fused with the KF algorithm. Chin J Aeronaut 2018;31(1):31–40.
[16] Yang Z, Wang Y, Kong C. Remaining useful life prediction of lithium-ion batteries based on a mixture of ensemble empirical mode decomposition and GWO-SVR model. IEEE Trans Instrum Meas 2021;70:1–11.
[17] Zhang C, Zhao S, He Y. An integrated method of the future capacity and RUL prediction for lithium-ion battery pack. IEEE Trans Veh Technol 2021;71(3):2601–13.
[18] Chen Z, Shi N, Ji Y, Niu M, Wang Y. Lithium-ion batteries remaining useful life prediction based on BLS-RVM. Energy 2021;234:121269.
[19] Zraibi B, Okar C, Chaoui H, Mansouri M. Remaining useful life assessment for lithium-ion batteries using CNN-LSTM-DNN hybrid method. IEEE Trans Veh Technol 2021;70(5):4252–61.
[20] Liu H, Liu Z, Jia W, Lin X. Remaining useful life prediction using a novel feature-attention-based end-to-end approach. IEEE Trans Ind Inform 2020;17:1197–207.
[21] Yang Y. A machine-learning prediction method of lithium-ion battery life based on charge process for different applications. Appl Energy 2021;292(5):116897.
[22] Li P, Zhang Z, Grosu R, Deng Z, Hou J, Rong Y, et al. An end-to-end neural network framework for state-of-health estimation and remaining useful life prediction of electric vehicle lithium batteries. Renew Sustain Energy Rev 2022;156:111843.
[23] Lu J, Xiong R, Tian J, Wang C, Hsu C-W, Tsou N-T, et al. Battery degradation prediction against uncertain future conditions with recurrent neural network enabled deep learning. Energy Storage Mater 2022;50:139-151.
[24] Tong Z, Miao J, Tong S, Lu Y. Early prediction of remaining useful life for lithium-ion batteries based on a hybrid machine learning method. J Cleaner Prod 2021;317:128265.
[25] Ma G, Zhang Y, Cheng C, Zhou B, Yuan Y. Remaining useful life prediction of lithium-ion batteries based on false nearest neighbors and a hybrid neural network. Appl Energy 2019;253:113626.
[26] Hu X, Che Y, Lin X, Deng Z. Health prognosis for electric vehicle battery packs: A data-driven approach. IEEE/ASME Trans Mech 2020;25(6):2622–32.
[27] Zhang Q, Yang L, Guo W, Qiang J, Peng C, Li Q, et al. A deep learning method for lithium-ion battery remaining useful life prediction based on sparse segment data via cloud computing system. Energy 2022;241:122716.
[28] Chen D, Meng J, Huang H, Wu J, Liu P, Lu J, et al. An empirical-data hybrid driven approach for remaining useful life prediction of lithium-ion batteries considering capacity diving. Energy 2022;245:123222.
[29] Tian J, Xiong R, Shen W, Lu J, Yang X-G. Deep neural network battery charging curve prediction using 30 points collected in 10 min. Joule 2021;5(6):1521–34.
[30] Cheng G, Wang X, He Y. Remaining useful life and state of health prediction for lithium batteries based on empirical mode decomposition and a long and short memory neural network. Energy 2021;232:121022.
[31] Huang NE, Shen Z, Long SR, Wu MC, Shih HH, Zheng Q, et al. The empirical mode decomposition and the Hilbert spectrum for nonlinear and non-stationary time series analysis. Proc Math Phys Eng Sci 1998;454(1971):903–95.
[32] Cho K, Van Merriënboer B, Gulcehre C, Bahdanau D, Bougares F, Schwenk H, et al. Learning phrase representations using RNN encoder-decoder for statistical machine translation. 2014, arXiv preprint arXiv:1406.1078.
[33] LeCun Y, Bengio Y, Hinton G. Deep learning. Nature 2015;521(7553):436–44.
[34] Chen Z, Chen L, Shen W, Xu K. Remaining useful life prediction of lithium-ion battery via a sequence decomposition and deep learning integrated approach. IEEE Trans Veh Technol 2021;71(2):1466–79.
[35] M. P. Battery data set. In: Center for advanced life cycle engineering CALCE. University of Maryland; 2011.
[36] Zhou D, Li Z, Zhu J, Zhang H, Hou L. State of health monitoring and remaining useful life prediction of lithium-ion batteries based on temporal convolutional network. IEEE Access 2020;8:53307–20.
[37] Pan D, Li H, Wang S. Transfer learning-based hybrid remaining useful life prediction for lithium-ion batteries under different stresses. IEEE Trans Instrum Meas 2022;71:1–10.
[38] Tang T, Yuan H. A hybrid approach based on decomposition algorithm and neural network for remaining useful life prediction of lithium-ion battery. Reliab Eng Syst Saf 2022;217:108082.
[39] Liu D, Luo Y, Liu J, Peng Y, Guo L, Pecht M. Lithium-ion battery remaining useful life estimation based on fusion nonlinear degradation AR model and RPF algorithm. Neural Comput Appl 2014;25:557–72.
[40] Zhou Y, Huang M. Lithium-ion batteries remaining useful life prediction based on a mixture of empirical mode decomposition and ARIMA model. Microelectron Reliab 2016;65:265–73.